JCI The Journal of Clinical Investigation

# Angiotensin II–dependent TGF-β signaling contributes to Loeys-Dietz syndrome vascular pathogenesis

Elena M. Gallo, … , David L. Huso, Harry C. Dietz

*J Clin Invest.* 2014;124(1):448-460. https://doi.org/10.1172/JCI69666.

**Research Article**

Loeys-Dietz syndrome (LDS) is a connective tissue disorder that is characterized by a high risk for aneurysm and dissection throughout the arterial tree and phenotypically resembles Marfan syndrome. LDS is caused by heterozygous missense mutations in either TGF-β receptor gene (*TGFBR1* or *TGFBR2*), which are predicted to result in diminished TGF-β signaling; however, aortic surgical samples from patients show evidence of paradoxically increased TGF-β signaling. We generated 2 knockin mouse strains with LDS mutations in either *Tgfbr1* or *Tgfbr2* and a transgenic mouse overexpressing mutant *Tgfbr2*. Knockin and transgenic mice, but not haploinsufficient animals, recapitulated the LDS phenotype. While heterozygous mutant cells had diminished signaling in response to exogenous TGF-β in vitro, they maintained normal levels of Smad2 phosphorylation under steady-state culture conditions, suggesting a chronic compensation. Analysis of TGF-β signaling in the aortic wall in vivo revealed progressive upregulation of Smad2 phosphorylation and TGF-β target gene output, which paralleled worsening of aneurysm pathology and coincided with upregulation of TGF-β1 ligand expression. Importantly, suppression of Smad2 phosphorylation and TGF-β1 expression correlated with the therapeutic efficacy of the angiotensin II type 1 receptor antagonist losartan. Together, these data suggest that increased TGF-β signaling contributes to postnatal aneurysm progression in LDS.



 Related Commentary, page 79

# Angiotensin II–dependent TGF-β signaling contributes to Loeys-Dietz syndrome vascular pathogenesis

Elena M. Gallo,[1] David C. Loch,[1] Jennifer P. Habashi,[1,2] Juan F. Calderon,[1] Yichun Chen,[1] Djahida Bedja,[3] Christel van Erp,[1] Elizabeth E. Gerber,[1] Sarah J. Parker,[1] Kimberly Sauls,[4] Daniel P. Judge,[5] Sara K. Cooke,[1] Mark E. Lindsay,[1] Rosanne Rouf,[1,5] Loretha Myers,[1] Colette M. ap Rhys,[1] Kathleen C. Kent,[1] Russell A. Norris,[4] David L. Huso,[6] and Harry C. Dietz[1,7]

[1]McKusick-Nathans Institute of Genetic Medicine, [2]Division of Pediatric Cardiology, Department of Pediatrics, and [3]Department of Molecular and Comparative Pathobiology, Johns Hopkins University School of Medicine, Baltimore, Maryland, USA. [4]Department of Regenerative Medicine and Cell Biology, Cardiovascular Developmental Biology Center, Children's Research Institute, Medical University of South Carolina, Charleston, South Carolina, USA. [5]Division of Cardiology and [6]Department of Molecular and Comparative Pathobiology, Johns Hopkins University School of Medicine, Baltimore, Maryland, USA. [7]Howard Hughes Medical Institute, Bethesda, Maryland, USA.

**Loeys-Dietz syndrome (LDS) is a connective tissue disorder that is characterized by a high risk for aneurysm and dissection throughout the arterial tree and phenotypically resembles Marfan syndrome. LDS is caused by heterozygous missense mutations in either TGF-β receptor gene (*TGFBR1* or *TGFBR2*), which are predicted to result in diminished TGF-β signaling; however, aortic surgical samples from patients show evidence of paradoxically increased TGF-β signaling. We generated 2 knockin mouse strains with LDS mutations in either *Tgfbr1* or *Tgfbr2* and a transgenic mouse overexpressing mutant *Tgfbr2*. Knockin and transgenic mice, but not haploinsufficient animals, recapitulated the LDS phenotype. While heterozygous mutant cells had diminished signaling in response to exogenous TGF-β in vitro, they maintained normal levels of Smad2 phosphorylation under steady-state culture conditions, suggesting a chronic compensation. Analysis of TGF-β signaling in the aortic wall in vivo revealed progressive upregulation of Smad2 phosphorylation and TGF-β target gene output, which paralleled worsening of aneurysm pathology and coincided with upregulation of TGF-β1 ligand expression. Importantly, suppression of Smad2 phosphorylation and TGF-β1 expression correlated with the therapeutic efficacy of the angiotensin II type 1 receptor antagonist losartan. Together, these data suggest that increased TGF-β signaling contributes to postnatal aneurysm progression in LDS.**

## Introduction

Loeys-Dietz syndrome (LDS) is a connective tissue disorder with significant phenotypic overlap with Marfan syndrome (MFS) (1, 2). Patients with MFS and LDS typically share skeletal features, including long fingers, chest wall deformity, scoliosis, and joint laxity. Both syndromes also present with dural ectasia and mitral valve prolapse. While most patients with MFS or LDS typically present with early and progressive aortic root enlargement, patients with LDS uniquely show widespread arterial tortuosity and a high risk for aneurysm and dissection throughout the arterial tree (1, 2). Aortic dissection in LDS often occurs at vascular dimensions below thresholds recommended for surgical intervention in MFS (2). This complex and aggressive vascular pathology makes LDS difficult to manage surgically and highlights the need for the development of medical therapies.

LDS is caused most often by heterozygous mutations in the gene encoding either the TGF-β receptor type I (*TGFBR1*) or TGF-β receptor type II (*TGFBR2*) subunit (TβRI and TβRII, respectively) (1–3). Most of these mutations, which substitute conserved amino acids in the serine/threonine kinase domain, are missense (1, 2). Receptors carrying LDS mutations fail to propagate signaling when expressed in cells naive for the corresponding subunit. Cotransfection of equal amounts of wild-type and mutant receptors results in approximately 50% reduction in TGF-β signaling output (3, 4), indicating that the mutant receptors are unable to propagate signal even in the presence of their wild-type counterpart.

Human genetics and animal studies have provided strong evidence for the involvement of the TGF-β pathway in aortic aneurysm. Upon TGF-β ligand binding to TβRII, TβRI (also known as ALK5) is recruited to and phosphorylated by TβRII. This event activates TβRI, which propagates signaling through phosphorylation of the receptor-regulated Smads (R-Smads), Smad2 and Smad3. Upon activation, R-Smads form heteromeric complexes with the Co-Smad, Smad4, and shuttle into the nucleus, in which they regulate expression of target genes (5). Our studies of both MFS mouse models and patients with MFS have shown that fibrillin-1 contributes to regulation of TGF-β signaling and that many manifestations of MFS, including aortic aneurysm (6–8), can be linked to overactivation of the TGF-β signaling pathway. Significantly, aortic root aneurysm in a Marfan mouse model could be attenuated by pharmacological antagonism of the TGF-β signaling pathway (8). A role for TGF-β signaling in aortic aneurysm has also been confirmed by the discovery that heterozygous inactivating mutations in genes encoding both positive (*SMAD3* and *TGFB2*) and negative effectors (*SKI*) of this pathway cause aneurysmal disorders very similar to LDS (9–11). These findings have caused con-

**Authorship note:** Elena M. Gallo and David C. Loch contributed equally to this work.

**Conflict of interest:** The authors have declared that no conflict of interest exists.

**Citation for this article:** *J Clin Invest.* 2014;124(1):448–460. doi:10.1172/JCI69666.

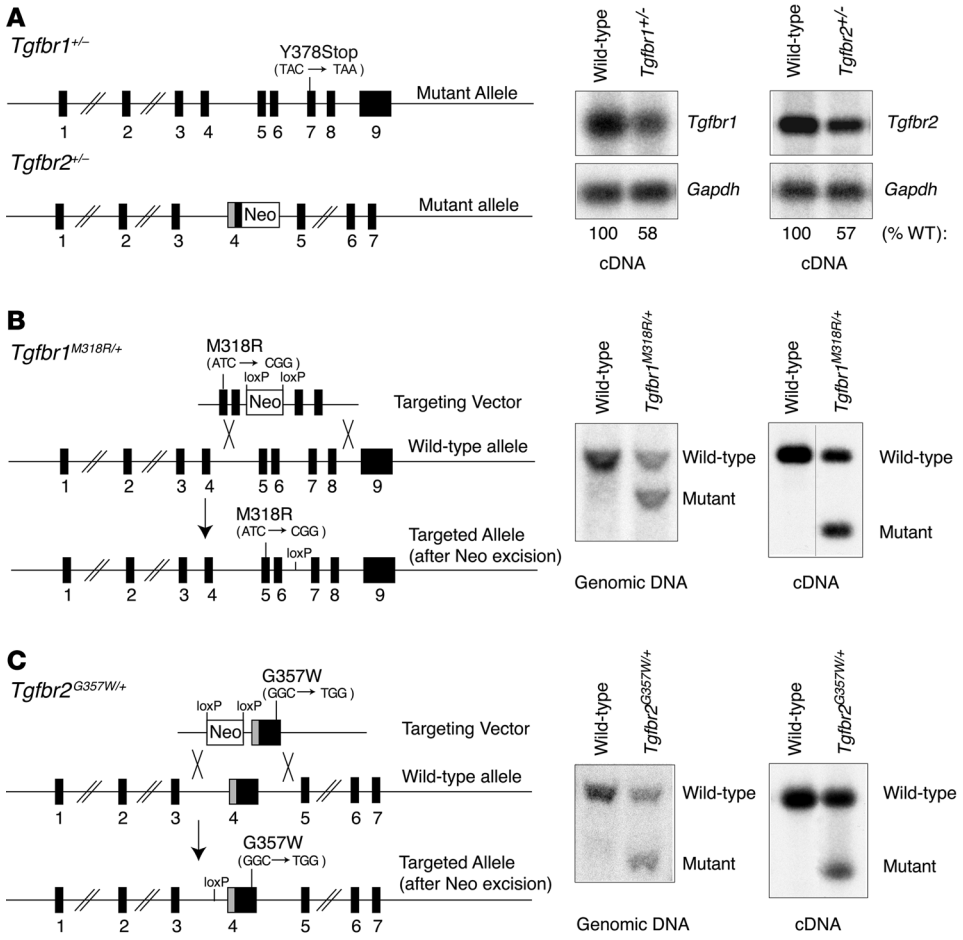


**Figure 1**
Mouse models of TGF-β receptor haploinsufficiency and LDS. (**A**) Structure of *Tgfbr1* and *Tgfbr2* mutant alleles in haploinsufficient mouse models. A stop mutation is present in exon 7 of the *Tgfbr1* mutant allele; a NeoR replaces part of exon 4 in the *Tgfbr2* mutant allele, creating a frameshift. These alterations result in an approximately 50% reduction in expression of the corresponding cDNA in aortic tissue derived from $Tgfbr1^{+/-}$ and $Tgfbr2^{+/-}$ haploinsufficient mice, as assessed by RT-PCR and indicated underneath the blots. (**B**) Structure of the $Tgfbr1^{M318R}$ mutant allele. ES cell targeting was verified by Southern blot. Expression of the mutant cDNA in aortic tissue derived from $Tgfbr1^{M318R/+}$ mice was verified by RT-PCR. *NciI* restriction digest allows for discrimination of wild-type and mutant cDNA (the black line indicates lanes that were run on the same gel but were noncontiguous). (**C**) Schematic illustrating the genomic structure of the $Tgfbr2^{G357W}$ mutant allele. ES cell targeting was verified by Southern blot. Expression of the mutant cDNA in aortic tissue derived from $Tgfbr2^{G357W/+}$ mice was evaluated by RT-PCR. *AlwI* restriction digest allows for discrimination of wild-type and mutant cDNA.

troversy regarding whether excessive or diminished activation of the TGF-β pathway is the primary driver of aortic root aneurysm (12, 13). In this light, the therapeutic use of agents with known TGF-β–suppressive properties, such as the angiotensin II type 1 receptor blocker (ARB) losartan (14), has remained controversial despite evidence for efficacy in MFS (8). To address these issues, we have developed and characterized mouse models of LDS and tested the therapeutic potential of losartan.

## Results

*TGF-β receptor knockin LDS mouse models, but not haploinsufficient mice, recapitulate LDS.* In transfection studies, LDS mutant receptor subunits fail to propagate signaling (3). It is therefore possible that loss of function of one allele of either TGF-β receptor gene might be sufficient to cause LDS. We therefore analyzed 2 mouse lines heterozygous for null alleles for either *Tgfbr1* or *Tgfbr2* and compared their phenotype to that of mice in which LDS-associated missense mutations were introduced in the endogenous genomic locus (Figure 1A). Both $Tgfbr1^{+/-}$ and $Tgfbr2^{+/-}$ mice showed an approximately 50% reduction in the expression of the corresponding TGF-β receptor transcript in the aortic wall when compared with that of wild-type littermates (Figure 1A). Mouse models that genetically mimic LDS were generated by targeting 2 missense mutations, which cause classic and severe manifestations of LDS in patients (1, 2), to their respective endogenous locus in either the *Tgfbr1* (M318R) or *Tgfbr2* (G357W) gene. Heterozygous mice resulting from homologous recombination are designated $Tgfbr1^{M318R/+}$ and $Tgfbr2^{G357W/+}$, respectively (Figure 1, B and C). RT-PCR and restriction digest of the PCR product confirmed approximately equal expression of the mutant and wild-type alleles in the aortic walls of heterozygous animals (Figure 1, B and C). Comparison of these 4 mouse strains revealed that mice carrying heterozygous missense LDS mutations, but not mice haploinsufficient for TGF-β receptor alleles, phenotypically recapitulate LDS. Aortic root size and growth in $Tgfbr1^{+/-}$ and $Tgfbr2^{+/-}$ mice was similar to that observed in wild-type mice, while $Tgfbr1^{M318R/+}$ and $Tgfbr2^{G357W/+}$ mice showed enlarged aortas and accelerated aortic root growth (Figure 2, A and B, and Supplemental Figure 1, A and B; supplemental material available online with this article; doi:10.1172/JCI69666DS1). Aortic root enlargement in both $Tgfbr1^{M318R/+}$ and $Tgfbr2^{G357W/+}$ mice progressively worsened between 4 and 24 weeks of age, with subtle but significant deviation from wild-type mice detectable at 4 weeks but highly reproducible and dramatic deviation at 24 weeks of age (Supplemental Figure 1). At 24 weeks of age, elastic fiber fragmentation was detectable in the aortic roots of LDS knockin mice but not in those of haploinsufficient strains (Figure 2, C and D). The aortic wall also showed progressive thickening with excessive collagen deposition in LDS mice (Supplemental Figure 1C). Both $Tgfbr1^{M318R/+}$ and $Tgfbr2^{G357W/+}$ mice, but not haploinsufficient animals, showed elongation and tortuosity of the aortic arch and coronary arteries as well as predisposition for aortic dissection and early death (hemothorax or

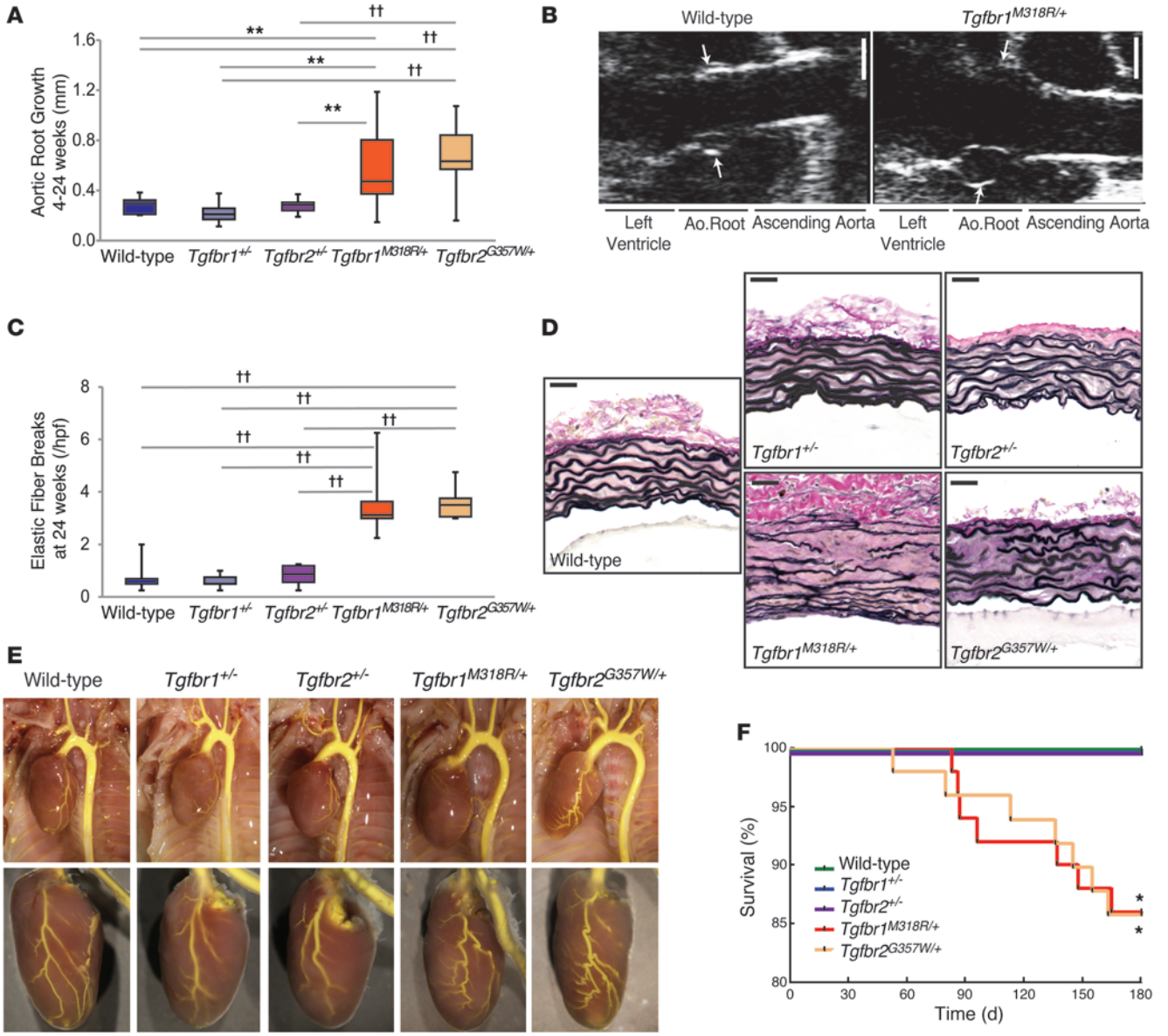


**Figure 2**

Knockin LDS mutant mice, but not TGF-β receptor haploinsufficient mice, recapitulate vascular LDS phenotypes. (**A**) Aortic root growth from 4 to 24 weeks of age in LDS knockin and haploinsufficient mouse models, as measured by echocardiography ($n \geq 9$). (**B**) Representative echocardiographic images of the aortic roots (arrows) of wild-type and *Tgfbr1*$^{M318R/+}$ mice at 24 weeks of age. Scale bar: 1 mm. (**C**) Quantification of elastic fiber breaks per high-power field (hpf) in LDS knockin and haploinsufficient mouse models ($n \geq 6$). (**A** and **C**) The upper and lower margins of the box define the 75th and 25th percentiles, respectively; the internal line defines the median, and the whiskers define the range. (**D**) Representative aortic wall sections of LDS knockin and haploinsufficient mouse models, at 24 weeks of age, stained with VVG for elastin. Scale bar: 40 μm. (**E**) Representative images of vascular anatomy in LDS knockin and haploinsufficient mouse models. (**F**) Kaplan-Meier survival curve showing diminished life span of *Tgfbr1*$^{M318R/+}$ and *Tgfbr2*$^{G357W/+}$ mice but not haploinsufficient mice (wild-type, $n = 46$; *Tgfbr1*$^{+/-}$, $n = 39$; *Tgfbr2*$^{+/-}$, $n = 32$; *Tgfbr1*$^{M318R/+}$, $n = 50$; *Tgfbr2*$^{G357W/+}$, $n = 49$). $^{*}P < 0.05$, $^{**}P < 0.005$, $^{\dagger\dagger}P < 0.00005$.

hemopericardium was observable in approximately 60% of deaths) (Figure 2, E and F). Knockin mice uniquely showed craniofacial and skeletal manifestations of LDS (Supplemental Figure 2, A and B). These findings indicate that haploinsufficiency for either TGF-β receptor gene is not sufficient to recapitulate LDS, while knockin LDS mouse models manifest many of the phenotypic features observed in patients.

*Transgenic overexpression of mutant Tgfbr2 recapitulates the vascular phenotype of LDS.* The absence of phenotype in mice haploinsufficient for TGF-β receptor, but recapitulation of pathology in knockin LDS mice, suggests that the presence of mutant TGF-β receptor protein is necessary to cause disease. To test whether expression of a mutant receptor subunit was sufficient to cause LDS, we engineered transgenic mice to ubiquitously overexpress

either wild-type or mutant (G357W) TβRII (1x Tg-*Tgfbr2* and 1x Tg-*Tgfbr2*$^{GW}$ mice, respectively) (Figure 3A). Aortic tissue from both 1x Tg-*Tgfbr2* and 1x Tg-*Tgfbr2*$^{GW}$ mice showed similar amounts of endogenous and transgene-derived *Tgfbr2* transcript. A higher mutant-to-endogenous transcript ratio was observed when the mutant transgene was bred to homozygosity, generating 2x Tg-*Tgfbr2*$^{GW}$ mice (Figure 3B). Both hemizygous and homozygous mutant transgenic mice displayed typical LDS vascular pathology, including aortic root dilatation (Figure 3C), elastic fiber fragmentation (Figure 3D), and arterial tortuosity (Figure 3E), although 2x Tg-*Tgfbr2*$^{GW}$ mice showed a more severe phenotype than 1x Tg-*Tgfbr2*$^{GW}$ mice. Additionally, 2x Tg-*Tgfbr2*$^{GW}$ mutant transgenic mice also died prematurely (hemothorax or hemopericardium was observable in approximately 70% of cases) (Figure 3F). Control transgenic mice (1x Tg-*Tgfbr2* mice) resembled wild-type littermates and showed no evidence of aortic aneurysm, vascular tortuosity, or premature death (Figure 3, C–F).

*Defective TGF-β receptor signaling in aortic LDS VSMCs in vitro*. In order to analyze the signaling alterations caused by LDS mutations, we generated primary aortic VSMCs cultures derived from the roots and proximal ascending aortas of *Tgfbr2*$^{G357W/+}$, *Tgfbr2*$^{+/-}$, and 2x Tg-*Tgfbr2*$^{GW}$ mice. RNA analysis of *Tgfbr2*$^{G357W/+}$ VSMCs showed levels of *Tgfbr2* mRNA comparable to those in wild-type VSMCs (Supplemental Figure 3A). In addition, pyrosequencing analysis showed that about 50% of *Tgfbr2* mRNA expressed in *Tgfbr2*$^{G357W/+}$ VSMCs carried the G357W mutation (Supplemental Figure 3B). *Tgfbr2*$^{G357W/+}$ VSMCs also showed normal surface levels of TβRII (Supplemental Figure 3C). In order to confirm normal expression and trafficking of the mutant receptor to the cell surface, we also assessed TβRII expression in T47D cells (which normally lack expression of TβRII) transfected with constructs expressing wild-type and *Tgfbr2*$^{G357W}$ mRNA as well as a GFP from an internal ribosomal entry site (IRES) on the same transcript. Expression of TβRII in GFP$^{+}$ cells transfected with wild-type construct was comparable to that of cells transfected with the mutant construct (Supplemental Figure 3D). Taken together, these data suggest that the G357W mutation does not affect expression or surface presentation of the derived TβRII protein and are consistent with previous reports indicating that most LDS-causing mutations do not affect receptor trafficking or surface expression (4). A similar analysis conducted on *Tgfbr2*$^{+/-}$ and 2x Tg-*Tgfbr2*$^{GW}$ VSMCs showed that these cells have decreased and increased expression of *Tgfbr2* mRNA, respectively (Supplemental Figure 4A). Approximately 50% of *Tgfbr2* mRNA in 2x Tg-*Tgfbr2*$^{GW}$ VSMCs harbors the G357W mutation (Supplemental Figure 4B). Surface expression of TβRII protein correlated with *Tgfbr2* mRNA expression, with *Tgfbr2*$^{+/-}$ and 2x Tg-*Tgfbr2*$^{GW}$ VSMCs showing lower and higher levels of TβRII surface expression compared with control VSMCs, respectively (Supplemental Figure 4C).

*Tgfbr2*$^{G357W/+}$, *Tgfbr2*$^{+/-}$, and 2x Tg-*Tgfbr2*$^{GW}$ VSMCs were starved and then stimulated with 10 ng/ml or 1 ng/ml TGF-β1 for 1 hour prior to assessment of Smad2 phosphorylation (pSmad2) by Western blot analysis (Figure 4, A–C). Both *Tgfbr2*$^{G357W/+}$ and 2x Tg-*Tgfbr2*$^{GW}$ VSMCs showed reduced signaling capacity in the acute response to administered ligand, with a maximal and significant deviation from that of wild-type cells (~50% reduction) at lower concentrations of ligand, while haploinsufficient *Tgfbr2*$^{+/-}$ VSMCs showed normal signaling. A similar reduction in pSmad2 was observed in human VSMCs derived from patients with LDS at the time of aortic surgery (Supplemental Figure 5A).

We next assessed the levels of pSmad2 in VSMCs grown in 5% serum at steady state. VSMCs derived from *Tgfbr2*$^{G357W/+}$ mice and from patients with LDS showed normal levels of pSmad2 when analyzed under these conditions (Figure 4D and Supplemental Figure 5B). In order to assess whether mutant VSMCs might compensate for their signaling deficiency by upregulation of TGF-β ligands, we measured their expression by qPCR. VSMCs derived from *Tgfbr2*$^{G357W/+}$ mice or patients with LDS showed either a trend toward increased expression of *Tgfb1* ($P$ = 0.09) or significant upregulation of *Tgfb2* under steady-state conditions when compared with control VSMCs, respectively (Figure 4E and Supplemental Figure 5C).

*Paradoxical overactivation of the TGF-β signaling pathway in the aortas of LDS mice*. The in vitro signaling experiments seemingly point to decreased TGF-β–dependent signaling, while we and others have observed increased signaling in aortic tissue samples from patients with LDS obtained at autopsy or surgery (1, 2, 9, 15). In this light, we monitored the status of TGF-β signaling in the proximal aortas of LDS mice at early and later stages of aneurysm development. Analysis of TGF-β signaling, as assessed by pSmad2 levels and expression of TGF-β target genes, showed apparently normal activation of this pathway in the aortic roots of LDS mice up to 8 weeks of age (Supplemental Figure 6). By 12 weeks of age, increased pSmad2 was observed in the aortic media of LDS mice when compared with that in wild-type littermates; this was most reliably monitored by in situ methods (such as immunofluorescence), as opposed to averaging techniques (i.e., immunoblot of tissue lysates), due to a variable but often intense proliferation and/or infiltration of cells within the adventitia of mutant mice (Figure 5B and Supplemental Figure 7, A and B). The increase in pSmad2 in the aortic media of LDS mice was further accentuated by 24 weeks of age (Figure 5C). Further analysis of the thickened and hyperplastic aortic root adventitia in LDS mice revealed infiltration of CD45$^{+}$ (bone marrow–derived) cells (Supplemental Figure 7C). Both CD45$^{+}$ adventitial cells and CD45$^{-}$ medial cells showed enhanced pSmad2 when compared with wild-type littermates (Figure 5D); adventitial cells also showed higher levels of total Smad2 (Supplemental Figure 7C). At this age, we also detected increased ERK phosphorylation (pERK) in the medial layer of the LDS aortic root (Supplemental Figure 8). This signaling profile correlated with increased expression of *Tgfb1* and collagen (Figure 6, A and B).

*Losartan prevents aortic aneurysm in LDS mutant mice*. Many of the phenotypic features of MFS that overlap with LDS, such as aortic root aneurysm, correlate with dysregulated TGF-β signaling and can be prevented by ARB therapy in mouse models (8, 16). We therefore tested whether the ARB losartan was an effective therapy in LDS mice. Mice were treated with hemodynamically equivalent oral doses (Supplemental Figure 9) of either losartan or the β-adrenergic receptor blocker propranolol from 4 weeks to 24 weeks of age. Losartan normalized aortic root growth and prevented deterioration of aortic wall architecture in LDS mice (Figure 7). The therapeutic efficacy of losartan correlated with reduced levels of pSmad2 and pERK in the medial layers of LDS mice (Figure 8A and Supplemental Figure 10). Propranolol had no effect on aortic root growth or aortic wall architecture (Figure 7) and failed to restore a normal signaling profile (Figure 8A and Supplemental Figure 10). In addition to reducing pSmad2, losartan treatment also normalized expression of *Tgfb1* and *Col1a1* and prevented cellular infiltration into the adventitia (Figure 8). In an

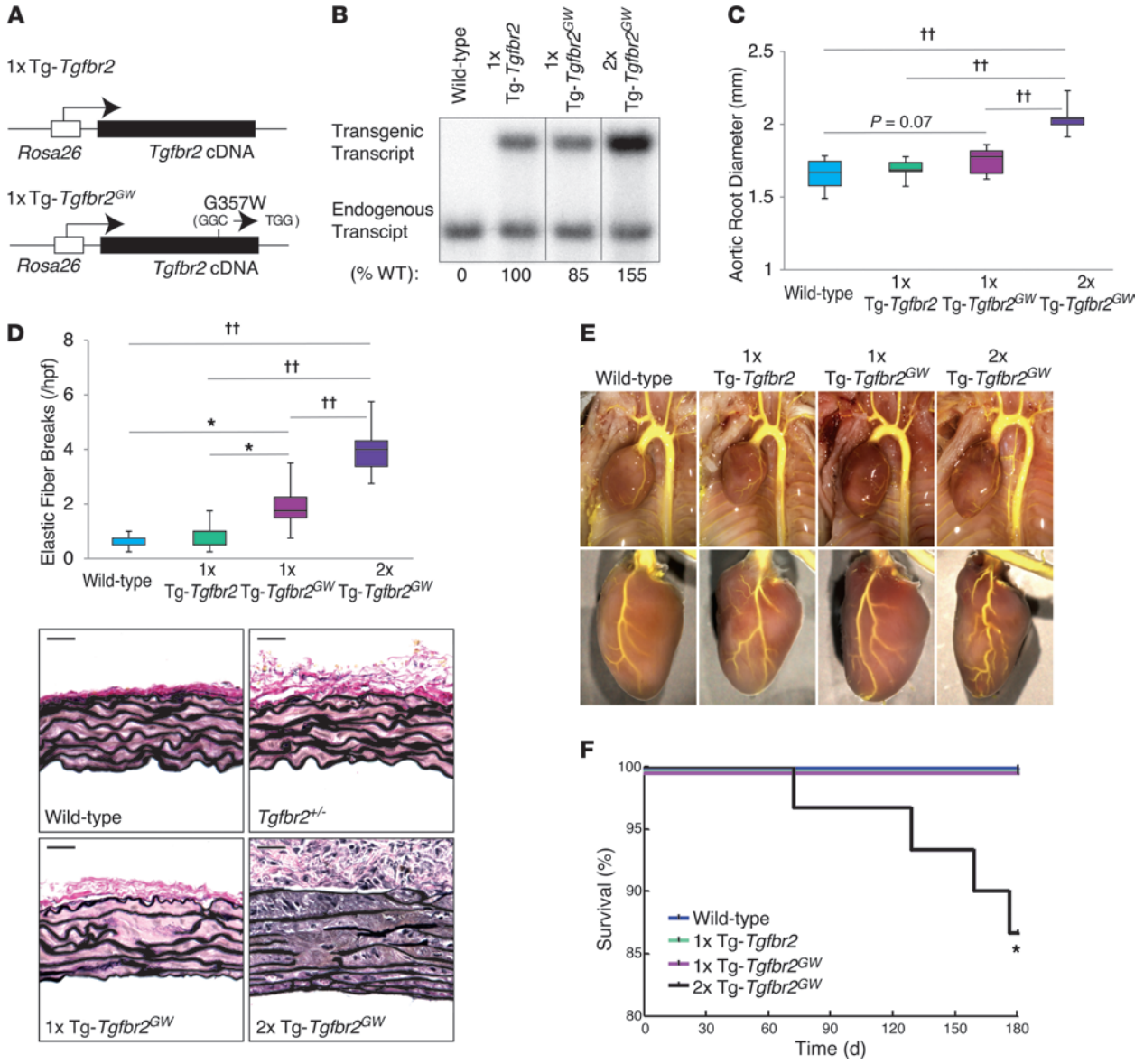


**Figure 3**

Transgenic mice overexpressing the *Tgfbr2*$^{G357W}$ mutant allele recapitulate vascular LDS phenotypes. (**A**) Schematic representation of control (1x Tg-*Tgfbr2*) and mutant (1x Tg-*Tgfbr2*$^{GW}$) transgenic constructs, both under the control of the *Rosa26* promoter. (**B**) Expression of endogenous and transgenic cDNA in aortic tissue of 1x Tg-*Tgfbr2*, 1x Tg-*Tgfbr2*$^{GW}$, and control mice, as evaluated by RT-PCR and indicated underneath the blots. After digestion with the restriction enzyme *MfeI*, which cuts the transgenic (both control and mutant) but not the endogenous cDNA, the PCR product was incubated with a radioactive probe specific for the *Tgfbr2* cDNA (the black lines indicate lanes that were run on the same gel but were noncontiguous). (**C**) Aortic root diameter of 24-week-old mice, as measured by echocardiography ($n \geq 6$). (**D**) Quantification of elastin fiber breaks per high-power field in control and mutant transgenic mice ($n \geq 6$) and representative VVG-stained aortic root sections from 24-week-old wild-type and transgenic mice. (**C** and **D**) The upper and lower margins of the box define the 75th and 25th percentiles, respectively; the internal line defines the median, and the whiskers define the range. Scale bar: 40 μm. (**E**) Representative images of vascular anatomy in control and transgenic mouse models. (**F**) Kaplan-Meier survival curve showing reduced life span for 2x Tg-*Tgfbr2*$^{GW}$ mice but not for 1x Tg-*Tgfbr2* and 1x Tg-*Tgfbr2*$^{GW}$ mice (wild-type, $n = 25$; 1x Tg-*Tgfbr2*, $n = 23$; 1x Tg-*Tgfbr2*$^{GW}$, $n = 26$; 2x Tg-*Tgfbr2*$^{GW}$, $n = 30$). $^{*}P < 0.05$, $^{††}P < 0.00005$.

attempt to directly assess the role of TGF-β in aneurysm progression in LDS mice, we performed a third trial with the pan-specific TGF-β–neutralizing monoclonal antibody (NAb) 1D11. The 1D11 NAb had only a modest effect in attenuating elastic fiber fragmentation in LDS mice and had no effect on aortic root dilatation (Supplemental Figure 11, A–C). Failure of the 1D11 NAb to rescue the aortic phenotype in LDS correlated with its failure to reduce pSmad2 in the aortic root media (Supplemental Figure 10A and Supplemental Figure 11D). Of note, LDS mice treated with the 1D11 NAb were chronically ill and died prematurely with severe cachexia in association with pronounced gastrointestinal inflammation but no aortic dissection.

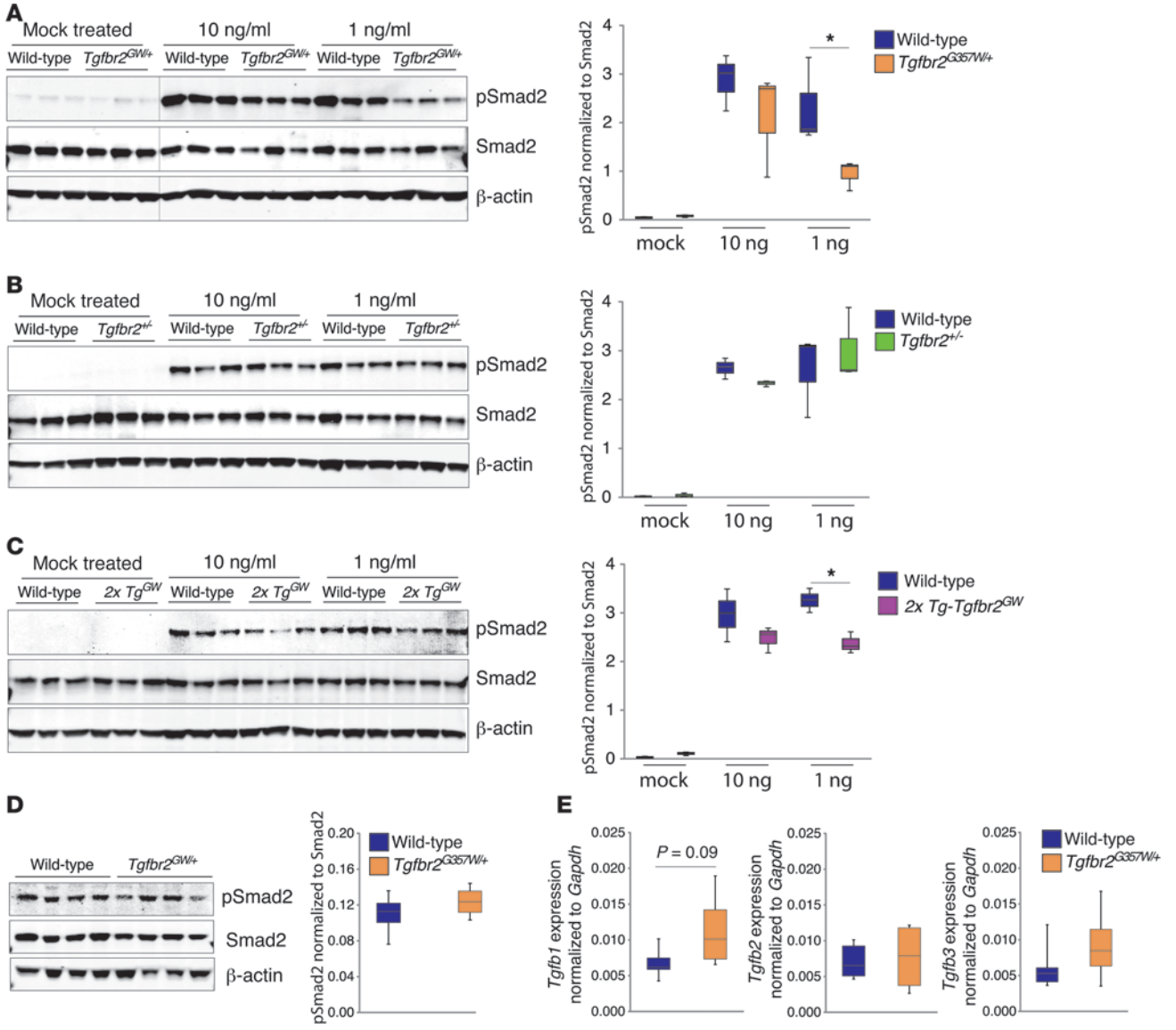


**Figure 4**
Defective TGF-β receptor signaling in LDS VSMCs in response to exogenous ligand but not under normal culture conditions. (**A**) Aortic VSMCs derived from wild-type and *Tgfbr2*$^{G357W/+}$ mice were starved for 24 hours in 2% serum and then exposed to 10 or 1 ng/ml TGF-β1 for 1 hour. Signaling events were assayed by Western blot (the black line indicates lanes that were run on the same gel but were noncontiguous) ($n$ = 3). (**B**) Western blot analysis of wild-type and *Tgfbr2*$^{+/-}$ VSMCs stimulated as in **A** ($n$ = 3). (**C**) Western blot analysis of wild-type and 2x Tg-*Tgfbr2*$^{GW}$ VSMCs stimulated as in **A** ($n$ = 3). (**D**) Levels of pSmad2 in unstimulated control and *Tgfbr2*$^{G357W/+}$ VSMCs grown in 5% serum to approximately 80% confluence prior to analysis ($n$ = 4). (**E**) Analysis of *Tgfb1*, *Tgfb2*, and *Tgfb3* expression in control and *Tgfbr2*$^{G357W/+}$ VSMCs cultured as in **D** ($n$ = 4). The upper and lower margins of the box define the 75th and 25th percentiles, respectively; the internal line defines the median, and the whiskers define the range. *$P$ < 0.05.

## Discussion

In this study we show that mouse strains haploinsufficient for either *Tgfbr1* or *Tgfbr2* do not recapitulate LDS. This is not surprising given that the vast majority of LDS mutations are predicted to give rise to mutant receptor subunits that traffic to the surface and bind ligands but are unable to propagate signal (2). Indeed, heterozygous mutations in *TGFBR1* that prevent ligand-binding or induce nonsense-mediated mRNA decay cause autosomal dominant Ferguson-Smith disease, characterized by focal self-healing squamous epitheliomas due to somatic loss of the wild-type allele, but no features of LDS (17). VSMCs derived from haploinsufficient mice also show normal TGF-β signaling potential in culture, despite half the normal levels of receptor at the cell surface, suggesting that this degree of reduced expression is not limiting.

Such findings are apparently at odds with a traditional antimorphic effect in which mutant protein interferes with the function of its wild-type counterpart owing to direct physical association, a plausible scenario given that heterotetrameric TGF-β receptor

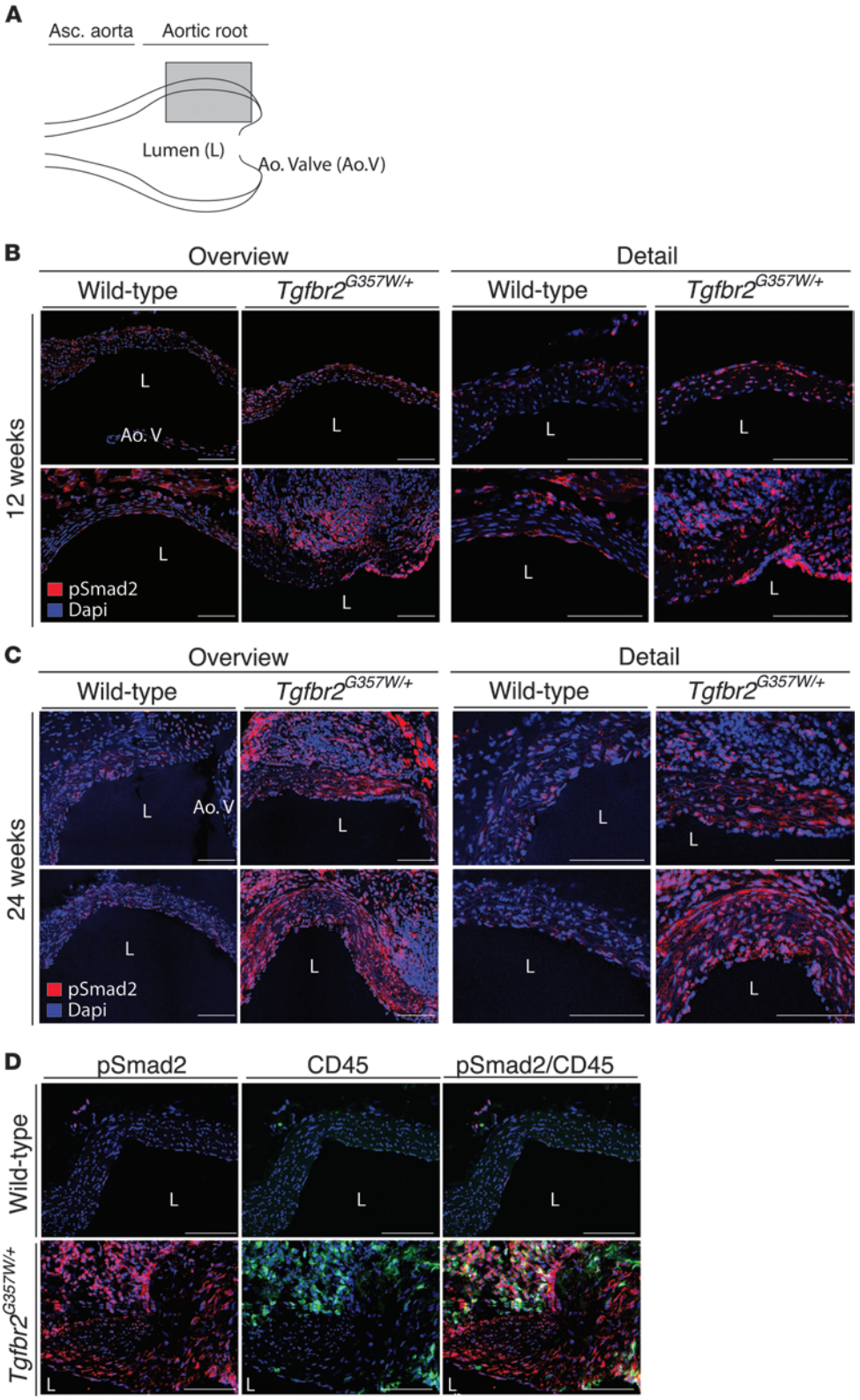


**Figure 5**
Progressive upregulation of pSmad2 in aortic tissue of LDS knockin mice. (**A**) Long-axis view used to acquire immunofluorescence images. The gray box indicates the approximate area used for imaging. Each image is shown at lower (overview) and higher (detail) resolution. (**B**) Representative images of pSmad2 in the aortic roots of 12-week-old *Tgfbr2*$^{G357W/+}$ and control mice. (**C**) Representative images of pSmad2 in the aortic roots of 24-week-old *Tgfbr2*$^{G357W/+}$ and control mice. (**D**) Representative images of pSmad2 and CD45 staining in the aortic roots of 24-week-old *Tgfbr2*$^{G357W/+}$ and control mice. Images were acquired as a tile with a ×25 magnification. Scale bar: 100 μm.

complexes are composed of 2 TβRI and 2 TβRII subunits (5). In this circumstance, it would be predicted that 3 out of 4 receptor complexes would lack the ability to propagate signal in the heterozygous state. In contrast, if each TβRI/TβRII dimer within the heterotetramer binds ligand and signals independently, as recently proposed (18), then half of the dimers would retain full signaling potential in heterozygous cells. In this scenario, one would predict normal signaling in the presence of high levels of

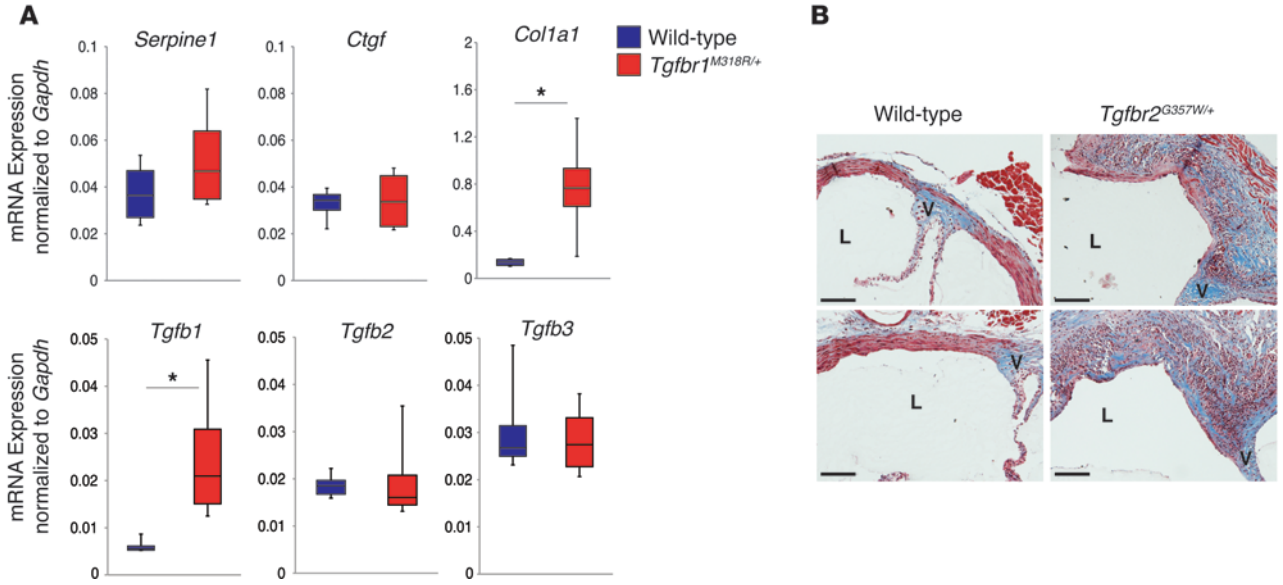


**Figure 6**

Upregulation of TGF-β1 ligand and collagen in LDS mice at 24 weeks of age. (**A**) Expression of TGF-β ligands and TGF-β gene targets in aortic root samples from 24-week-old *Tgfbr1*$^{M318R/+}$ mice, as evaluated by qPCR ($n$ = 4). The upper and lower margins of the box define the 75th and 25th percentiles, respectively; the internal line defines the median, and the whiskers define the range. *$P$ < 0.05. (**B**) Masson trichrome staining of representative sections of the aortic roots of control and *Tgfbr2*$^{G357W/+}$ mice at 24 weeks of age. L, lumen; V, aortic valve annulus. Scale bar: 200 μm.

ligand (as seen in haploinsufficient cells), with a maximal signaling reduction of 50% when mutant and wild-type dimers compete for a limiting amount of ligand. This mechanistic hypothesis appears to best match our observations.

Demonstration of a decline in TGF-β signaling potential by LDS VSMCs in vitro, albeit conditional and relative, still offers the null hypothesis that vascular disease in LDS is simply driven by low TGF-β signaling, a view apparently supported by the finding that other LDS-like phenotypes are caused by heterozygous loss-of-function mutations in genes encoding positive effectors of TGF-β signaling, including *SMAD3* and *TGFB2* (9, 10). However, a number of observations make this position difficult to defend. First, the phenotypic overlap between LDS and MFS, a condition consistently associated with high TGF-β signaling, is undeniable (13). Second, many studies have documented a tissue signature for high TGF-β signaling in the aortic walls of patients with LDS (caused by mutations in *TGFBR1*, *TGFBR2*, *SMAD3*, or *TGFB2*) during phases of postnatal aneurysm progression, and no study has provided evidence for low TGF-β signaling in LDS in vivo (1, 9, 10, 15). Third, Shprintzen-Goldberg syndrome, a condition that includes virtually every manifestation of LDS, is caused by mutations in or near the Smad binding domain of SKI (a potent inhibitor of TGF-β signaling) — an event predicted and observed to cause high TGF-β signaling (11).

Our analysis of the aortic tissue of LDS mice has failed to detect any evidence of impaired signaling but rather showed increased levels of pSmad2 and TGF-β target gene expression, which are detectable by 12 weeks of age and progressively accentuate with worsening of the disease. Importantly, the striking protection afforded by losartan correlates with reduced pSmad2 and TGF-β ligand expression within both the adventitial and medial compartments. While apparently normal TGF-β signaling was observed at 8 weeks of age despite evolving evidence of aneurysms, young mice remained responsive to losartan; this could reflect either lack of sensitivity of our assays to subtle perturbations in TGF-β signaling or an independent influence of angiotensin II signaling at this age.

It remains possible that some LDS phenotypes might in fact be caused by a simple decrease in TGF-β signaling. In support of this notion, some of the phenotypic manifestations in LDS, such as cleft palate, have been associated with abrogation of TGF-β signaling in mice (19, 20). This would also explain the susceptibility of LDS mice treated with TGF-β–neutralizing antibody to overt gastrointestinal inflammation, a known TGF-β deficiency phenotype in mice (21, 22).

Despite this progress, a number of issues remain. First, what is the mechanism for the paradoxically enhanced signaling, and, second, why did TGF-β–neutralizing antibody fail to afford protection in LDS mice? We observe no in vitro evidence for a cell-autonomous gain of function for mutant TGF-β receptor subunits. Rather, cell culture and in vivo studies suggest that chronic compensatory events may contribute to maintenance or enhancement of TGF-β signaling by LDS cells, respectively. It seems notable that tissue from patients or mice with various etiologies of LDS, including mutations in *SMAD3* and *TGFB2*, shows increased expression of TGF-β1 (9, 10). The high TGF-β1 expression seen in LDS could lead to enhanced TGF-β signaling due to the absolute amount of ligand being expressed and/or the contribution of alternative activators of TGF-β, such as integrins, which contribute to activation of TGF-β1 but not TGF-β2 (23). The specific source of TGF-β1 in LDS has not been fully explored. We previously proposed that specific cell types that are particularly vulnerable to the impaired function imposed by heterozygous LDS mutations might attempt to compensate for this deficiency by secreting excessive amounts of TGF-β ligand into their immediate

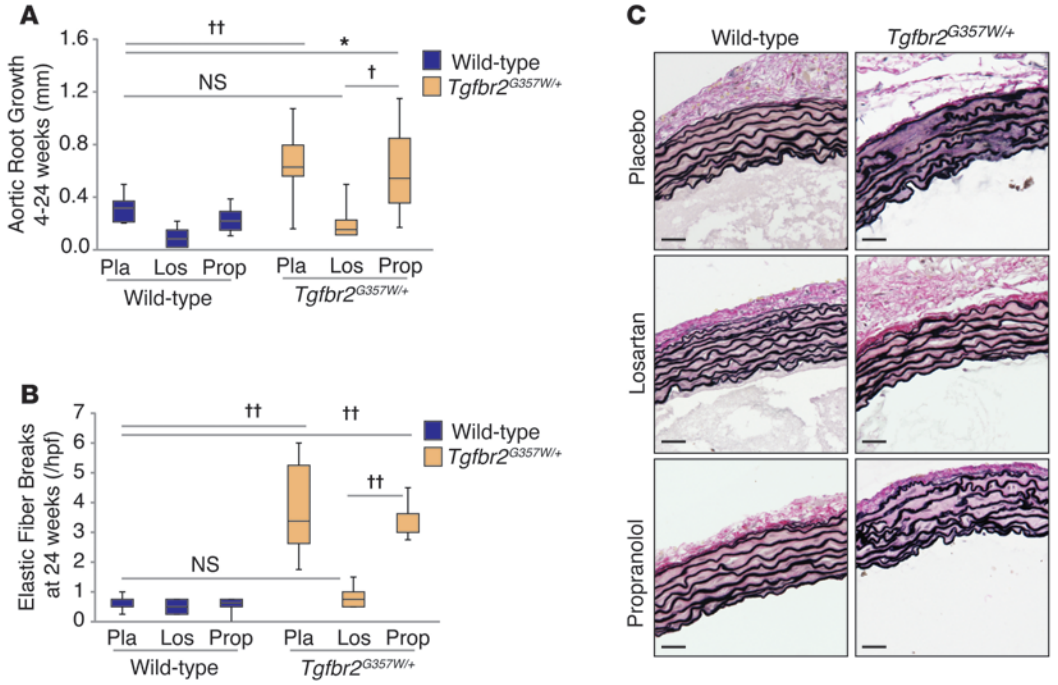


**Figure 7**

Treatment with the angiotensin II receptor 1 inhibitor losartan ameliorates LDS vascular pathology. (**A**) Aortic root growth from 4 to 24 weeks of age, as measured by echocardiography, in *Tgfbr2*$^{G357W/+}$ and control mice treated with placebo, propranolol, or losartan ($n \geq 8$). (**B**) Elastic fiber breaks per high-power field in *Tgfbr2*$^{G357W/+}$ and control mice treated with placebo, propranolol, or losartan ($n \geq 8$). (**A** and **B**) The upper and lower margins of the box define the 75th and 25th percentiles, respectively; the internal line defines the median, and the whiskers define the range. (**C**) VVG staining of representative sections of the proximal ascending aortas of *Tgfbr2*$^{G357W/+}$ and control mice treated with placebo, propranolol, or losartan. Scale bar: 40 μm. $^{*}P < 0.05$, $^{\dagger}P < 0.0005$, $^{\dagger\dagger}P < 0.00005$.

environment (13). This could lead to paracrine overdrive of TGF-β signaling in neighboring cells, with relatively preserved signaling capacity despite expression of mutant receptors. In the aortic root, the 2 critical cell populations might be second heart field– and neural crest–derived VSMCs (13, 24, 25). Additionally, infiltrating CD45$^{+}$ cells, whose presence correlates with the severity of the aneurysm pathology, might also contribute to signaling overdrive.

In contrast to MFS, in which TGF-β–neutralizing antibody suppressed TGF-β signaling and afforded relative but significant protection (8, 26), this reagent neither improved nor accentuated aortic pathology and had no effect on TGF-β signaling in LDS mice. While 1D11 is described as a pan-specific TGF-β–neutralizing antibody, it is possible that it has differential effects on the various TGF-β ligands and that the predominant ligand underlying LDS pathology is relatively resistant. In addition, systemically delivered 1D11 might have limited capacity to penetrate the overtly thickened, collagen-rich, and hypercellular LDS vessel wall, as previously proposed for hypertrophic cardiac tissue (27). Alternatively, an excess of pSmad2 may relate to an accentuation of other pathways capable of mediating this event, such as angiotensin II or activin signaling (28, 29); both could remain responsive to losartan.

LDS is associated with aggressive and diffuse vascular disease, with involvement of arterial segments that are difficult to approach surgically. While it is clear that the pathogenesis of LDS is complex and requires additional study and refinement, we provide critical preclinical evidence for the use of ARBs in the treatment of LDS. Hemodynamically equivalent doses of the beta-blocker propranolol, which lowers blood pressure but does not affect Smad2 signaling, failed to preserve aortic wall architecture and had only a modest effect on the rate of aortic root dilation. This suggests that losartan-dependent amelioration of pathologic aortic growth and medial degeneration is not solely dependent on its antihypertensive properties and might in fact depend on its ability to circumvent or suppress whatever mechanism is driving excessive TGF-β signaling in LDS mice. The therapeutic efficacy of losartan in the treatment of aortic disease in LDS mice suggests that therapies developed for MFS may find broader application in additional inherited disorders of vessel wall homeostasis.

## Methods

*Mice*. *Tgfbr1*$^{+/-}$ mice were generated by chemical mutagenesis by Ingenium and obtained from The Jackson Laboratory. These mice harbor a nonsense mutation in exon 7 (cytosine to adenine at nucleotide 1134). *Tgfbr2*$^{+/-}$ mice (30) were provided by Makoto Taketo (Kyoto University, Kyoto, Japan). For the generation of *Tgfbr1*$^{M318R/+}$ and *Tgfbr2*$^{G357W/+}$ mice, murine genomic fragments of *Tgfbr1* (9 kb, exons 5–8) and *Tgfbr2* (8.4 kb, exon 4) were obtained by long-range PCR of 129S6/SvEvTac ES cell DNA. Both were separately subcloned into plasmid pSL301 (Life Technologies). Site-directed mutagenesis was performed using the QuikChange Mutagenesis Kit (Stratagene), substituting arginine for methionine at codon 318 of *Tgfbr1* and substituting tryptophan for glycine at codon 357 of *Tgfbr2*. A neomycin resistance cassette (NeoR) was amplified from pEGFP-C1 (Life Technologies) using PCR primers with the loxP sequence flanking either end by AgeI linkers (*Tgfbr1*) or BamHI linkers (*Tgfbr2*). Each of the floxed NeoR amplicons were

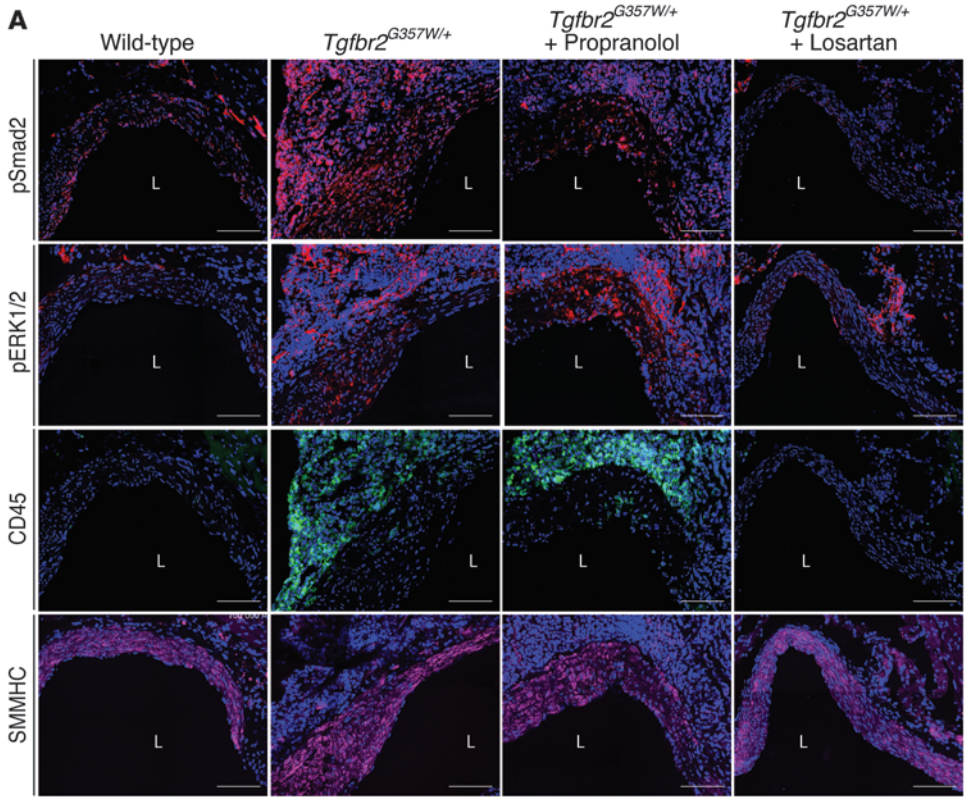


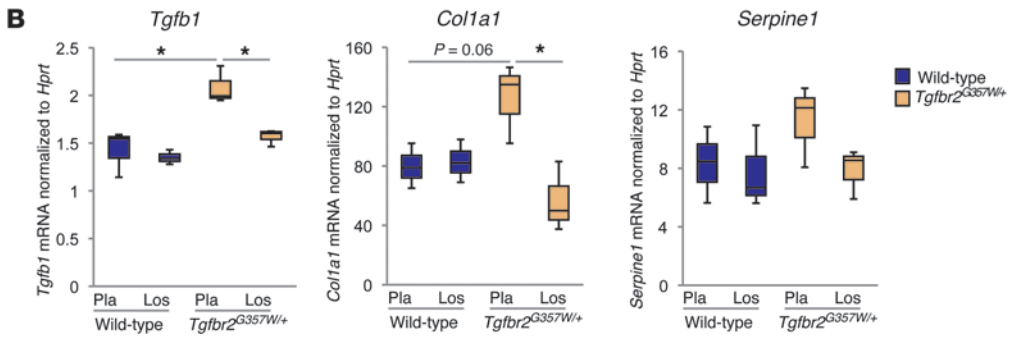


**Figure 8**
Amelioration of LDS vascular pathology by losartan treatment correlates with inhibition of pSmad2 and decreased expression of TGF-β ligand. (**A**) Representative images of pSmad2, pERK1/2, CD45, and smooth muscle myosin heavy chain (SMMHC) staining in the aortic roots of 24-week-old *Tgfbr2*$^{G357W/+}$ and control mice treated with placebo, propranolol or losartan. Images were acquired as a tile with a ×25 magnification. Scale bar: 100 μm. (**B**) Expression of *Tgfb1*, *Col1a1*, and *Serpine1* in aortic root samples from 24-week-old *Tgfbr2*$^{G357W/+}$ and control mice treated with placebo (Pla) or losartan (Los) ($n$ = 3). The upper and lower margins of the box define the 75th and 25th percentiles, respectively; the internal line defines the median, and the whiskers define the range. *$P$ < 0.05.

then separately subcloned into pCR2.1-TOPO (Life Technologies). AgeI and BamHI digestion fragments containing the NeoR and flanking loxP sequences were ligated into either a unique Age1 site in *Tgfbr1* intron 6–7 or a unique BamHI site in *Tgfbr2* intron 3–4. Both vectors were linearized by a unique restriction site (XmaI and AgeI for *Tgfbr1* and *Tgfbr2*, respectively) prior to electroporation into 129S6/SvEvTac ES cells by the Johns Hopkins Transgenic Core Facility. Positive clones were identified by Southern blot analysis. Briefly, Southern probes derived from genomic DNA 5′ and 3′ to the targeting vector were designed to recognize the insertion of a novel NcoI site in the NeoR. Sequencing of 5′ and 3′ long-range PCR products from the NeoR to outside the targeting construct confirmed proper targeting. Positive clones were injected into C57BL6/J blastocysts at E3.5 and transferred into pseudopregnant females by the Johns Hopkins Transgenic Core Facility. Chimeric offspring were mated to C57BL6/J mice, and germline transmission was confirmed by RT-PCR and restriction digest. The loxP-flanked NeoR was removed by mating *Tgfbr1*$^{M318R/+}$ and *Tgfbr2*$^{G357W/+}$ founder mice with CAG-Cre recombinase transgenic mice (31). Experimental mice were backcrossed onto a 129S6/SvEvTac background at least 5 times. Wild-type littermates were used as controls. For the generation of 1x Tg-*Tgfbr2* and 1x Tg-*Tgfbr2*$^{GW}$ transgenic mice, murine *Tgfbr2* cDNA was cloned into pBROAD3 vector (Invivogen). This plasmid enables ubiquitous transgene expression in transgenic mice by virtue of its *ROSA26* promoter. For the mutant *Tgfbr2* transgenic mouse, site-directed mutagenesis was performed using the QuikChange Mutagenesis Kit (Stratagene), substituting tryptophan for glycine at codon 357 as described above. Both vectors were linearized by PacI digestion prior to pronuclear injection into C57B6/SJL $F_1$ embryos by the Johns Hopkins Transgenic Core Facility. Founder mice were confirmed by Southern blot analysis. Transgenic mice were backcrossed at least 4 times onto a C57B6 background prior to experimentation. Wild-type littermates were used as controls. All constructs were validated by Sanger sequencing. All animal experiments were approved by the Johns Hopkins Animal Care and Use Committee.

*Tissue processing for RNA and protein extraction*. For RNA extraction, tissue was processed using the RNeasy Fibrous Tissue Kit (Qiagen) or TRIzol (Life Technologies) plus an automatic bead homogenizer (FastPrep24, MP Biomedicals). In all cases, an on-column DNAse digest was performed

using RNeasy mini columns (Qiagen). Protein was extracted using the Total Protein Extraction Kit (Millipore) and a pestle motor (Kimble-Kontes) or using an automatic bead homogenizer in conjunction with reagents from the Protein Extraction Kit (Full Moon Biosystems). All protein lysis buffers contained protease and phosphatase inhibitors (Millipore).

*RT-PCR and quantification of transcript expression*. Transcript levels for the gene or transgene of interest were determined by RT-PCR, followed by incubation with a radioactive probe specific for the corresponding cDNA, or by amplification with prevalidated TaqMan probes. For quantification with radioactive probes, cDNA was generated with the SuperScript III First-Strand Synthesis System (Life Technologies) using oligo-dT primers. A PCR of 25 cycles was then performed on the resultant cDNA with primers specific for the cDNA of interest. After electrophoresis, the PCR products were Southern blot transferred to a membrane and subsequently hybridized with a $^{32}$P-γ–dATP–labeled oligonucleotide from the original PCR using UltraHyb (Ambion). Relative quantification was determined using a phosphoimager. Differential restriction patterns were exploited to discriminate between mutant and endogenous transcripts. An *NciI* restriction and an *AlwI* restriction site are introduced by the M318R mutation and the G357W mutation, respectively, in the corresponding mutant cDNA; a *MfeI* site is present in the endogenous *Tgfbr2* cDNA but not in the transgenically expressed control or mutant cDNA. For cDNA quantification using prevalidated TaqMan probes, cDNA was generated using TaqMan High-Capacity cDNA Reverse Transcription reagents. Quantitative PCR was performed in triplicate with TaqMan Universal PCR Master Mix using an ABI Prism 7900HT QPCR machine (all from Applied Biosystems). The following prevalidated TaqMan probes were used to detect specific transcripts: Mm99999915_g1 (Gapdh), Mm01545399_m1 (Hprt), Mm01178820_m1 (Tgfb1), Mm00436955_m1 (Tgfb2), Mm00436960_m1 (Tgfb3), Mm00801666_g1 (Col1a1), Mm01192932_g1 (Ctgf), and Mm00435860_m1 (Serpine1). For human samples, the following probes were used: Hs00998133_m1 (Tgfb1), Hs00234244_m1 (Tgfb2), Hs01086000_m1 (Tgfb3), and Rn01775763_g1 (Gapdh). Reactions were run in triplicate, and relative quantification for each transcript was obtained by normalizing against housekeeping control transcript.

*Aortic histology*. Following halothane-induced euthanasia, the abdominal and chest walls were dissected away, the left common iliac artery was transected to facilitate drainage, and the left ventricle was then flushed with 5 ml PBS (pH 7.4). Approximately 2 ml yellow latex (Ward's Natural Science) was injected directly into the apex of the left ventricle. Mice were then kept moist at 4°C for 3 to 4 hours to facilitate setting of the injected latex. Whole mice were subsequently fixed overnight in 10% neutral buffered formalin (Fisher Scientific) and then stored in 70% ethanol prior to performance of dissections. The heart and thoracic aorta were dissected out en bloc. Transverse sections (~3 mm long) of the entire thoracic aorta (root, ascending, transverse, and descending segments) were mounted in 4% agar prior to paraffin embedding. Five-micron sections were stained with Verhoeff–van Gieson (VVG) for elastin and with Movat or Masson trichrome for collagen. Slides were examined using an Eclipse E400 microscope (Nikon Inc.). The number of elastic fiber breaks per high power field was calculated from VVG-stained aortic sections. For each genotype, age, and treatment group, entire aortic rings (with many high-power fields per ring) were analyzed at 4 distinct sites of the aortic root and proximal ascending aorta. Genotype and treatment groups were determined only after this analysis was concluded.

*Alcian blue– and Alizarin red–stained skeletons*. Mice were first euthanized by halothane inhalation then skinned and eviscerated. Carcasses were then sequentially placed in 95% ethanol for 2 days, Alcian blue staining solution (0.015% Alcian Blue 8X [Sigma-Aldrich], 80% ethanol, 20% acetic acid) for 10 days, 95% ethanol for 2 days, 1% potassium hydroxide for 4 days to facilitate tissue clearing, and Alizarin red staining solution (0.001% Alizarin Red [Sigma-Aldrich] in 1% potassium hydroxide) for 3 days. Whole skeleton photography was performed by the Pathology Photography and Computer Graphic Department of Johns Hopkins.

*Generation of primary aortic VSMC cultures and TGF-β stimulation*. For murine samples, aortic VSMC cultures were established from roots and proximal ascending aortas of 8-week-old mice. Aortas were digested in 300 U/ml collagenase II (Worthington Biochemical Corp.) in HBSS (Life Technologies) for 10 minutes at 37°C to facilitate removal of the endothelium and adventitia. Following an overnight incubation in DMEM (Life Technologies) with 20% FBS, aortas were washed with HBSS and digested with 300 U/ml collagenase II and 3 U/ml elastase for 45 minutes at 37°C. Aortas were triturated with a Pasteur pipette and incubated with DMEM plus 20% FBS. Four days were allowed for the VSMCs to adhere to the plate, after which the media was changed to DMEM plus 10% FBS. Human aortic VSMC cultures were established from aortic root samples obtained at surgery. After removal of the adventitial and intima layer, a "clean" piece of media was minced into small pieces and SmGM-2 media (Lonza, product CC-3182) was added to the dish. Cells growing out of the pieces of tissue were grown to approximately 80% confluence prior to freezing and/or further experiments. Control human ascending aorta VSMCs were obtained from Lonza and PromoCell. For stimulation experiments, murine and human aortic VSMC cultures were grown to approximately 80% confluence in 10% DMEM or SmGM-2 media (Lonza, product CC-3182), respectively. Cultures were then starved in 2% DMEM or SmBm-2 media (Lonza, product CC-3182) for 24 hours before the addition of recombinant human TGF-β1 (R&D Systems, product 240-B-010) or vehicle. For "steady-state" studies, VSMCs were grown in SmGM-2 media (Lonza, product CC-3182) to approximately 80% confluence. Protein lysates were harvested and lysed in M-PER buffer (Pierce) plus protease and phosphatase inhibitors (Millipore).

*Flow cytometry*. VSMCs were grown to approximately 70% confluence in DMEM plus 10% FBS. Cultures were then starved in 2% serum for 24 hours before analysis. Cells were lifted from culture plates by adding ice-cold 0.5 mM EDTA for 10 minutes, washed twice with PBS, and then resuspended in PBS containing 0.5% BSA (Flow Cytometry Staining Buffer). Cells were stained with APC-conjugated anti-mouse TβRII antibody (R&D Systems, FAB532A) or APC-conjugated isotype control antibody (R&D Systems, IC108A) by adding 10 μl of antibody to $10^6$ cells in 100 μl. Cells were incubated for 60 minutes on ice in the dark. Unbound antibody was removed by washing the cells in Flow Cytometry Staining Buffer twice. Stained cells were then fixed for 10 minutes at room temperature in 4% PFA in PBS, washed with Flow Cytometry Staining Buffer, and resuspended in 1 ml Flow Cytometry Staining Buffer prior to acquisition. Flow cytometry data were acquired on a BD FACSVerse flow cytometer (BD Biosciences). Results were evaluated, including median fluorescent intensity calculations, using FlowJo software (Tree Star Inc.).

*Generation of Tgfbr2-IRES-GFP constructs and transfection of T47D cells*. *Tgfbr2* cDNA was obtained from Open Biosystems (Thermo Scientific) and cloned into a pIRES2-AcGFP1 vector (Clontec); site-directed mutagenesis (QuikChange II XL Site-Directed Mutagenesis Kit, Stratagene, Agilent Technologies) was used to introduce the G357W mutation in the *Tgfbr2*$^{WT}$-IRES-GFP construct and thus generate the *Tgfbr2*$^{G357W}$-IRES-GFP construct. T47D cells were obtained from ATCC. Transfection was performed using Lipofectamine 2000 (Invitrogen, Life Technologies) according to the manufacturer's protocol. Cells were grown to approximately 90% confluence prior to transfection. GFP and TβRII expression was assayed 24 hours after transfection.

*Western blotting*. Western blotting was performed using LI-COR buffer and species-appropriate secondary antibodies conjugated to IRdye-700 or IRdye-800 (LI-COR Biosciences), according to the manufacturer's

guidelines, and analyzed using LI-COR Odyssey. The following primary antibodies were used: anti-phospho Smad2 (Millipore, clone A5S), anti-GAPDH (Abcam, Ab9483), anti-actin (Sigma-Aldrich, clone AC-74), anti-Smad2 (Cell Signaling Technology, 3103), anti-phospho Erk1/2 (Cell Signaling Technology, 4370), anti-phospho p38 (Cell Signaling Technology, 4511), and anti-phospho JNK (Cell Signaling Technology, 9251).

*Immunofluorescence on frozen aortic tissue sections*. Mice were euthanized by halothane inhalation. Following sacrifice, the abdominal and chest walls were dissected away and the left common iliac artery was transected to facilitate drainage. The left ventricle was then flushed with 20 ml PBS (pH 7.4) and then approximately 20 ml PBS containing 4% paraformaldehyde. The heart and thoracic aorta were then dissected out en bloc and fixed in fresh 4% paraformaldehyde in PBS at 4°C overnight. The following day, tissue blocks were immersed in antigen retrieval solution (10 mM sodium citrate buffer, pH 6.0) at 4°C overnight and then immersed in boiling antigen retrieval solution for 3 minutes. Tissue was then immediately placed in cold 30% sucrose in PBS and incubated at 4°C overnight, embedded in Tissue-Tek O.C.T. Compound, and frozen using ethanol mixed with dry ice and stored at –80°C. Frozen 10-μm long-axis view ("candy cane") sections were obtained with a cryostat and mounted on glass slides. Sections were dried for at least 1 day at room temperature prior to staining. Sections were permeabilized in staining buffer (PBS containing 0.1% Triton-X 100) for 15 minutes and then incubated with Fc Receptor Block from Innnovex for 30 minutes at room temperature, washed briefly in staining buffer, and then incubated again in blocking solution (0.1% Triton-X 100, 1:50 goat serum, 0.3 M glycine) for 30 minutes. Primary antibodies were diluted at 1:100 in staining buffer and incubated overnight at 4°C. Three consecutive washes with staining buffer were performed prior to incubation with goat anti-rabbit secondary antibody conjugated to Alexa Fluor 594 (Life Technologies) at 1:200 for 1 hour. If double staining for the CD45 antigen was performed, slides were then incubated with anti-CD45 antibody overnight at 4°C and then again washed 3 times prior to mounting with VECTASHIELD Hard Set Mounting Media with DAPI. Images were acquired on Zeiss AxioExaminer with 710NLO-Meta multiphoton confocal microscope at a ×25 magnification. The following primary antibodies were used: anti-phosho Smad2 (Millipore, clone A5S), anti-phospho ERK1/2 (Cell Signaling Technology, 4370), anti-Smad2 (Abcam, Ab33875), anti–pan-leukocyte marker CD45–Alexa Fluor 488 (Biolegend, 103121), and anti–smooth muscle myosin heavy chain (Abcam, ab53219).

*Drug treatment*. Losartan (100 mg/kg) and propranolol (80 mg/kg) dosing was performed daily by oral gavage or by administration of losartan food diet (Harlan) designed to deliver 3 mg drug per day (8). The mouse monoclonal antibody against TGF-β1, TGF-β2, and TGF-β3 (R&D Systems, clone 1D11) was given 3 times per week by intraperitoneal injection (5 mg/kg). Mice were treated from 4 to 24 weeks of age. Similar numbers of males and females were used in each treatment group.

*Plethysmography and echocardiography*. Blood pressures were measured by tail cuff plethysmography in the week prior to the completion of drug treatment. Mice were habituated to the system for 5 days, and, on the fifth day, 3–5 blood pressures were obtained and averaged. Echocardiograms were undertaken on conscious mice, whose hair had been removed with Nair cream, using Visualsonics Vevo 660 V1.3.6 imaging system (VisualSonics). Echocardiographic recordings were taken using a parasternal long-axis view; 3 independent measurements of the maximal internal dimension at the sinus of Valsalva were made and averaged. All imaging and measurements were performed by a cardiologist who was blinded to genotype and treatment arm.

*Statistics*. Data are presented as box-and-whiskers plots. The upper and lower margins of the box define the 75th and 25th percentiles, respectively; the internal line defines the median, and the whiskers define the range. For experiments including multiple comparisons, *P* values refer to 1-way ANOVA followed by Tukey's honestly significant difference (HSD) test. For experiments including only one comparison, *P* values refer to unpaired 2-tailed Student's *t* test. Survival curves were compared with log-rank (Mantel-Cox) test. $P \leq 0.05$ was considered statistically significant.

*Study approval*. Patients were recruited from the Connective Tissue Clinic at Johns Hopkins Hospital. Recovery of aortic tissue samples at surgery for the generation of primary VSCM cultures was performed in compliance with the Johns Hopkins School of Medicine Institutional Review Board and after informed consent.

## Acknowledgments

We thank Makoto Taketo for providing critical reagents. We thank N. Barker from the Pathology Photography and Computer Graphic Department of Johns Hopkins for photography of the mouse skeletons, the Johns Hopkins Transgenic Core Facility for assistance in generation of new mouse strains, and the Johns Hopkins Microscope Facility for assistance in acquisition of immunofluorescence images. This work was supported by NIH grant AR41135-18. H.C. Dietz is also supported by the Howard Hughes Medical Institute. E.M. Gallo was also supported by a Helen Hay Whitney Foundation postdoctoral fellowship.

Received for publication March 4, 2013, and accepted in revised form October 10, 2013.

Address correspondence to: Harry C. Dietz, Institute of Genetic Medicine, Johns Hopkins University School of Medicine, MRB 539, 733 N. Broadway, Baltimore, Maryland 21205, USA. Phone: 410.614.0701; Fax: 410.614.2256; E-mail: hdietz@jhmi.edu.

David C. Loch's present address is: Fisher Adam Kelly, Patent and Trademark Attorneys, Brisbane, Queensland, Australia.

Mark E. Lindsay's present address is: Massachusetts General Hospital Thoracic Aortic Center, Boston, Massachusetts, USA.

1. Loeys BL, et al. A syndrome of altered cardiovascular, craniofacial, neurocognitive and skeletal development caused by mutations in TGFBR1 or TGFBR2. *Nat Genet*. 2005;37(3):275–281.
2. Loeys BL, et al. Aneurysm syndromes caused by mutations in the TGF-beta receptor. *N Engl J Med*. 2006;355(8):788–798.
3. Mizuguchi T, et al. Heterozygous TGFBR2 mutations in Marfan syndrome. *Nat Genet*. 2004; 36(8):855–860.
4. Horbelt D, Guo G, Robinson PN, Knaus P. Quantitative analysis of TGFBR2 mutations in Marfan-syndrome-related disorders suggests a correlation between phenotypic severity and Smad signaling activity. *J Cell Sci*. 2010; 123(pt 24):4340–4350.
5. Shi Y, Massague J. Mechanisms of TGF-β signaling from cell membrane to the nucleus. *Cell*. 2003; 113(6):685–700.
6. Neptune ER, et al. Dysregulation of TGF-β activation contributes to pathogenesis in Marfan syndrome. *Nat Genet*. 2003;33(3):407–411.
7. Ng CM, et al. TGF-β-dependent pathogenesis of mitral valve prolapse in a mouse model of Marfan syndrome. *J Clin Invest*. 2004;114(11):1586–1592.
8. Habashi JP, et al. Losartan, an AT1 antagonist, prevents aortic aneurysm in a mouse model of Marfan syndrome. *Science*. 2006;312(5770):117–121.
9. van de Laar IM, et al. Mutations in SMAD3 cause a syndromic form of aortic aneurysms and dissections with early-onset osteoarthritis. *Nat Genet*. 2011;43(2):121–126.
10. Lindsay ME, et al. Loss-of-function mutations in TGFB2 cause a syndromic presentation of thoracic aortic aneurysm. *Nat Genet*. 2012;44(8):922–927.
11. Doyle AJ, et al. Mutations in the TGF-β repressor SKI cause Shprintzen-Goldberg syndrome with aortic aneurysm. *Nat Genet*. 2012; 44(11):1249–1254.
12. Wang Y, et al. TGF-β activity protects against inflammatory aortic aneurysm progression and complications in angiotensin II-infused mice.

*J Clin Invest*. 2010;120(2):422–432.
13. Lindsay ME, Dietz HC. Lessons on the pathogenesis of aneurysm from heritable conditions. *Nature*. 2011;473(7347):308–316.
14. Lavoie P, Robitaille G, Agharazii M, Ledbetter S, Lebel M, Lariviere R. Neutralization of transforming growth factor-beta attenuates hypertension and prevents renal injury in uremic rats. *J Hypertens*. 2005;23(10):1895–1903.
15. Gomez D, et al. Syndromic and non-syndromic aneurysms of the human ascending aorta share activation of the Smad2 pathway. *J Pathol*. 2009; 218(1):131–142.
16. Brooke BS, Habashi JP, Judge DP, Patel N, Loeys B, Dietz HC. Angiotensin II blockade and aortic-root dilation in Marfan's syndrome. *N Engl J Med*. 2008; 358(26):2787–2795.
17. Goudie DR, et al. Multiple self-healing squamous epithelioma is caused by a disease-specific spectrum of mutations in TGFBR1. *Nat Genet*. 2011; 43(4):365–369.
18. Huang T, et al. TGF-β signalling is mediated by two autonomously functioning TβRI:TβRII pairs. *EMBO J*. 2011;30(7):1263–1276.
19. Kaartinen V, et al. Abnormal lung development and cleft palate in mice lacking TGF-β 3 indicates defects of epithelial-mesenchymal interaction. *Nat Genet*. 1995;11(4):415–421.
20. Sanford LP, et al. TGFβ2 knockout mice have multiple developmental defects that are non-overlapping with other TGFβ knockout phenotypes. *Development*. 1997;124(13):2659–2670.
21. Monteleone G, Kumberova A, Croft NM, McKenzie C, Steer HW, MacDonald TT. Blocking Smad7 restores TGF-beta1 signaling in chronic inflammatory bowel disease. *J Clin Invest*. 2001;108(4):601–609.
22. Yang X, et al. Targeted disruption of SMAD3 results in impaired mucosal immunity and diminished T cell responsiveness to TGF-β. *EMBO J*. 1999; 18(5):1280–1291.
23. Munger JS, Sheppard D. Cross talk among TGF-β signaling pathways, integrins, and the extracellular matrix. *Cold Spring Harb Perspect Biol*. 2011;3(11):a005017.
24. Topouzis S, Majesky MW. Smooth muscle lineage diversity in the chick embryo. Two types of aortic smooth muscle cell differ in growth and receptor-mediated transcriptional responses to transforming growth factor-beta. *Dev Biol*. 1996; 178(2):430–445.
25. Cheung C, Bernardo AS, Trotter MW, Pedersen RA, Sinha S. Generation of human vascular smooth muscle subtypes provides insight into embryological origin-dependent disease susceptibility. *Nat Biotechnol*. 2012;30(2):165–173.
26. Holm TM, et al. Noncanonical TGFβ signaling contributes to aortic aneurysm progression in Marfan syndrome mice. *Science*. 2011;332(6027):358–361.
27. Koitabashi N, et al. Pivotal role of cardiomyocyte TGF-β signaling in the murine pathological response to sustained pressure overload. *J Clin Invest*. 2011;121(6):2301–2312.
28. Rodriguez-Vita J, Sanchez-Lopez E, Esteban V, Ruperez M, Egido J, Ruiz-Ortega M. Angiotensin II activates the Smad pathway in vascular smooth muscle cells by a transforming growth factor-β-independent mechanism. *Circulation*. 2005; 111(19):2509–2517.
29. Bernard DJ. Both SMAD2 and SMAD3 mediate activin-stimulated expression of the follicle-stimulating hormone β subunit in mouse gonadotrope cells. *Mol Endocrinol*. 2004;18(3):606–623.
30. Oshima M, Oshima H, Taketo MM. TGF-β receptor type II deficiency results in defects of yolk sac hematopoiesis and vasculogenesis. *Dev Biol*. 1996; 179(1):297–302.
31. Sakai K, Miyazaki J. A transgenic mouse line that retains Cre recombinase activity in mature oocytes irrespective of the cre transgene transmission. *Biochem Biophys Res Commun*. 1997;237(2):318–324.